Thermodynamic Study of a Water–Dimethylformamide–Polyacrylonitrile Ternary System

Lianjiang Tan,[1] Ding Pan,[1] Ning Pan[2]

[1]*State Key Laboratory for Chemical Fiber Modification and Polymer Materials, Donghua University, Shanghai 201620, People's Republic of China*
[2]*Biological and Agricultural Engineering Department, University of California, Davis, California 65616*

Received 23 October 2007; accepted 6 March 2008
DOI 10.1002/app.28392
Published online 15 September 2008 in Wiley InterScience (www.interscience.wiley.com).

ABSTRACT: Experimental cloud-point data were obtained by cloud-point titration. The phase diagram for a ternary system of water–dimethylformamide–polyacrylonitrile was determined by numerical calculation on the basis of the extended Flory–Huggins theory and was found to agree well with the cloud-point data. To construct the theoretical phase diagram, three binary interaction parameters were obtained with different methods. The ternary phase diagram was used to investigate the mechanism of fiber formation. The skin–core structure and fingerlike pores in polyacrylonitrile fiber may be effectively eliminated if the composition of the spinning solution is properly chosen, and consequently, homogeneous polyacrylonitrile fiber with a bicontinuous structure and good mechanical properties can be obtained through the spinning process. © 2008 Wiley Periodicals, Inc. J Appl Polym Sci 110: 3439–3447, 2008

Key words: fibers; mixing; phase behavior; thermodynamics

INTRODUCTION

Polyacrylonitrile (PAN) is soluble in many polar organic liquids, such as dimethylformamide (DMF), dimethyl sulfoxide, and dimethyl acetemide. PAN solutions with certain concentrations can be used as spinning solutions to produce precursor fibers for PAN-based carbon fibers, which largely determine the quality of PAN carbon fibers. The coagulation mechanism of PAN fibers during either wet spinning or dry-jet wet spinning is very complex because of the coexistence of double diffusion and phase separation. During the formation of an as-spun PAN fiber, the concentrated polymer solution is transformed into a gel structure through a series of steps that involve the mixing and demixing of the components under a variety of environmental conditions. Thus, it is clearly desirable to formulate a thermodynamic framework applicable to the initial stages of fiber formation and using a ternary phase diagram is deemed effective in this respect.

When the polymer concentration is low in a ternary system, its phase diagram can be constructed with the method of cloud-point titration.[1–11] At high polymer concentration, however, the interaction between macromolecules is so strong that the polymer solution shows signs of crystallization or becomes gel-like.[2–5] From our previous studies, we learned the ternary phase diagram of a PAN solution with a concentration over 8% could not be obtained through the cloud-point titration method. Because the concentration of PAN solution used for spinning is usually over 10%, the Flory–Huggins theory for such polymer solutions, also extended by Tompa[12] to ternary systems containing nonsolvent, solvent, and polymer, is needed to establish the phase diagram, including the binodal curve, spinodal curve, and critical point. In this study, a ternary system consisting of PAN, DMF, and water (H_2O), which is popular in the formation of PAN fibers, was investigated. Cloud-point titration was performed for PAN solutions with low concentrations to obtain the cloud-point curve, and the theoretical ternary phase diagram at a temperature of 25°C was numerically calculated. PAN fibers were spun from the PAN solutions with different amount of H_2O. The cross-section morphology and the mechanical properties of the fibers were studied. Some conclusions on thermodynamic problems of fiber formation were reached after carefully analysis of the results.

EXPERIMENTAL

Materials

PAN copolymers (acrylonitrile/itaconic acid = 98 : 2) were purchased from Shanghai Institute of Synthetic Fiber (Shanghai, China) with a weight-average

Correspondence to: D. Pan (dingpan@dhu.edu.cn).
Contract grant sponsor: National Basic Research Program (973 Program); contract grant number: 2006CB606505.
Contract grant sponsor: National Natural Science Foundation of China; contract grant number: 50333050.
Contract grant sponsor: Shanghai Fundamental Theory Program; contract grant number: 07DJ14002.
Contract grant sponsor: Specialized Research Fund for the Doctoral Program of Higher Education; contract grant number: 20020255010.

molecular weight of 8×10^4 g/mol. DMF (chemically pure) was purchased from Shanghai Chemical Reagent Co., Ltd. (Shanghai, China), and deionized H_2O was used as the nonsolvent.

Determination of the cloud-point curve

The cloud-point curve was determined by the titration method. For this purpose, PAN in DMF solutions with concentrations of 1, 2, 3, 4, 5, 6, and 7 wt % were prepared by the mixing of a required amount of PAN powder and DMF in a round-bottom flask sealed with a rubber septum stopper. The mixture was stirred by an electric paddle stirrer for 2 h at 50°C for swelling and for 5 h at 70°C for dissolving. During the titration process, the temperature of the mixture was controlled at 25°C with a thermostatic H_2O bath. Deionized H_2O was then introduced into the flask through the septum by a microsyringe while the stirrer was still working for a thorough mixing. At the first sight of turbidity, the addition of H_2O was stopped, and the cloudy solution was agitated for 10 min and then left still for another 10 min. More H_2O was added only when the solution became homogeneous again; otherwise, the determined point was considered as the onset of the cloud point. The composition of the cloud point was then determined by measurement of the amount of H_2O, DMF, and PAN present in the flask.

Preparation of the PAN solution

A certain amount of PAN copolymer was dispersed in the mixture of DMF and H_2O (the concentration of H_2O was 2 wt %) in a three-necked bottle. The existence of H_2O may accelerate the coagulation of the spinning solution for fiber or film preparation. The resulting slurry was allowed to swell at 50 and 60°C for 2 h each and was stirred by an electric paddle stirrer. Subsequently, it was further stirred at 70°C for 6 h to produce a viscous solution with 20 wt % PAN. Then, the solution was deaerated in a vacuum drying oven and kept at 70°C.

Equilibrium swelling

PAN films were prepared by a casting method with the PAN solution, six strips of 5×6 mm^2 PAN films, each with a weight of about 0.3 g and a thickness of 50–60 μm. The strips were immersed in an H_2O bath at constant temperature of 25°C. After 24 h, the strips were removed, passed between tissue paper, and weighed in a weighting bottle to get their wet weight [W_{wet} (g)]. Then, the wet strips were dried in a vacuum drying oven at 50°C for 12 h so that their dry weight [W_{dry} (g)] was also gained.

Fiber formation

Four 20 wt % PAN/DMF spinning solutions containing different amounts of H_2O (0, 1, 3, and 5 wt %) were prepared with the aforementioned method. Dry-jet wet spinning was used to form the as-spun PAN fibers. The dope was spurted at 70°C from a spinneret with a hole (diameter = 0.8 mm, length–diameter ratio = 10) and put into the coagulating bath with a DMF concentration of 50 wt % at 25°C. The air gap between the spinneret and the coagulating bath was 3 cm. The extrusion velocity was 10.3 m/min, and the linear velocity of the first winding roller was fixed at 20.6 m/min, so the draw ratio was 2.

Mechanical properties of the as-spun fibers

The mechanical properties of the as-spun PAN fibers were measured on an XQ-1 tensile-testing machine (custom made by Donghua University, China) under standard testing conditions (i.e., relative humidity = 65 ± 2%, temperature = 27 ± 2°C) with a crosshead speed of 10 mm/min at gauge length of 20 mm and an applied tension of 0.15 cN. In each case, 10 samples were tested, and the average values of tenacity and Young's modulus were obtained.

Cross-section morphology of the as-spun fibers

The cross sections of the as-spun fibers produced from the PAN solutions with different H_2O contents were made on a Hardy's thin cross-section sampling device. The micrographs of the cross sections were taken with a JSM-5600LV scanning electron microscope (made by Jeol, Tokyo, Japan).

RESULTS AND DISCUSSION

Cloud-point data

Figure 1 shows the cloud-point curve for the H_2O–DMF–PAN system, which was the experimental binodal curve denoting the border between the compositions that were completely stable, metastable, or unstable.

Determination of the thermodynamic parameters

To calculate a phase diagram numerically, a set of three binary interaction parameter values should be known. The analysis of the binary systems allowed us to apply physically realistic values of binary interaction parameters to the ternary system investigated in this study. In the following text, the subscripts 1, 2, and 3 refer to the nonsolvent, solvent, and polymer, respectively.

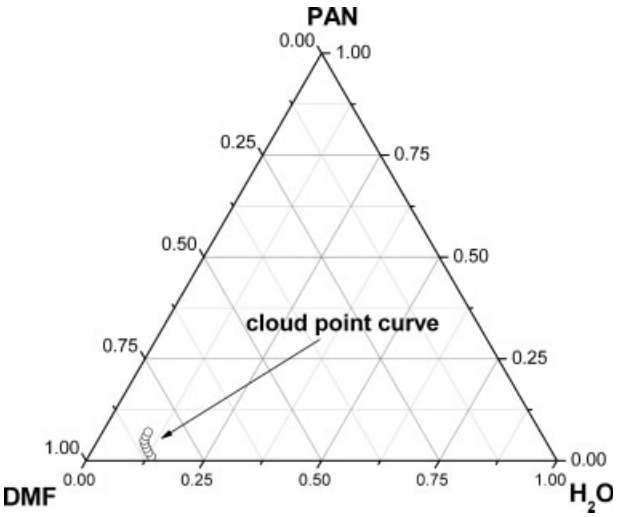

Figure 1 Cloud-point curve for the H_2O–DMF–PAN system.

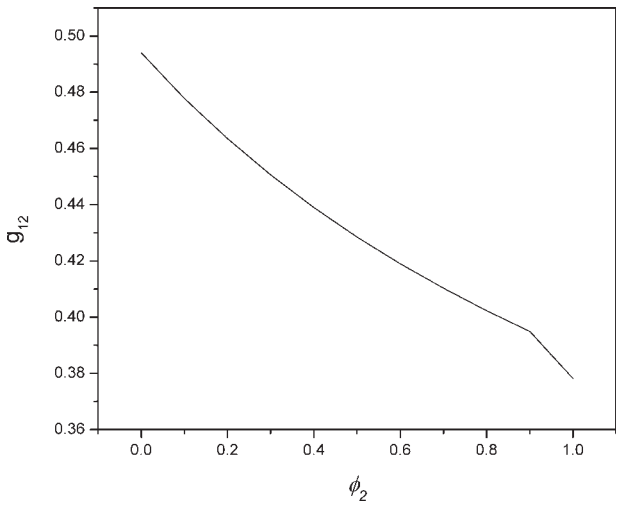

Figure 2 Relation between g_{12} and ϕ_2 (temperature = 25°C).

H_2O–DMF binary system

According to the literature,[13–16] the Flory–Huggins interaction parameters for several solvent–nonsolvent binary systems can be expressed by the following equation:

$$g_{12} = \alpha + \frac{\beta}{1 - \gamma\phi_2} \tag{1}$$

where g_{12} is a concentration-dependent interaction parameter of the H_2O–DMF system α, β, and γ are three parameters which differ for different binary systems, and ϕ_2 is the volume fraction of DMF. For an H_2O–DMF binary system at 25°C, the values of α, β, and γ are listed in Table I.[13] In this article, for the convenience of expression, g_{ij}, which represents interaction parameters, is used on all occasions whether the interaction parameters are concentration-dependent or not.

The relation between g_{12} and ϕ_2 in eq. (1) is illustrated in Figure 2. The value of g_{12} decreased with increased values of ϕ_2. In addition, in the whole range of the concentration of DMF, g_{12} was below 0.5, which indicated a strong polar interaction between H_2O and DMF. This was also verified by the heat produced when H_2O and DMF were mixed.

TABLE I
Three Parameters in eq. (1) for the H_2O/DMF Binary System

α	β	γ
0.218	0.276	−0.622

The data were taken from ref. 13.

H_2O–PAN binary system

To evaluate the interaction parameter of a nonsolvent–polymer (H_2O–PAN) binary system (g_{13}), several experimental techniques can be used, such as equilibrium swelling, adsorption, osmotic pressure, and light scattering.[17,18] Among these, the method of equilibrium swelling is simple and convenient as well as effective.

A polymer can be seen as a kind of swollen crosslinking network produced by entanglement and Van der Waals forces among macromolecular chains and crystalline regions. We used the Flory–Rehner theory to describe the swelling behavior of the polymer.[17] In the case that the nonsolvent does not interact strongly with the polymer, that is, the increment of polymer's weight after it is fully swollen is less than 30% of its initial weight, the elastic free enthalpy in the variation of free energy can be ignored, and we obtained the following equation:[17]

$$g_{13} = -\frac{\ln(1 - \phi 3) + \phi 3}{\phi 3^2} \tag{2}$$

where ϕ_3 is the volume fraction of the polymer.

Furthermore, for such an H_2O–PAN system, the volume fraction of the PAN copolymer (ϕ_3) was determined through measurement of the augment of the copolymer's weight after the swelling experiment:

$$\phi_3 = \frac{W_{dry}/\rho_{PAN}}{W_{wet} - W_{dry}/\rho_{water} + W_{dry}/\rho_{PAN}} \tag{3}$$

where ρ_{PAN} and ρ_{water} are the densities of the PAN copolymer and water, respectively.

Consequently, the interaction parameter g_{13} was obtained. The results of the experiments and calculations are listed in Table II.

TABLE II
Results of PAN–H_2O Swelling Experiments (Temperature = 25°C)

Experiment	W_{wet} (g)	W_{dry} (g)	ϕ_3	g_{13}
1	0.3458	0.3260	0.9353	2.061
2	0.3784	0.3062	0.9285	1.983
3	0.3133	0.2925	0.9250	1.946
4	0.3705	0.3513	0.9413	2.138
5	0.2883	0.2657	0.9116	1.822
6	0.3198	0.2973	0.9206	1.763

We took the average of the six values of g_{13} as the value to be used in the study, that is, $g_{13} = 1.95$.

DMF–PAN binary system

There are many approaches to determine the solvent–polymer (DMF–PAN) interaction parameter (g_{23}), such as osmotic pressure, light scattering,[19] and gas–liquid equilibrium.[20] Among these, usually the gas–liquid equilibrium is experimentally preferred.[20] However, the partial vapor pressure of DMF was so low (0.35kPa at 20°C) that this method became infeasible. We used a formula instead to evaluate g_{23}:[13]

$$g_{ij} = \frac{V_i}{RT}(\delta_i - \delta_j)^2 \tag{4}$$

where V_i is the molar volume of DMF, δ_i and δ_j are the solubility parameters of component i and component j, respectively, T is the absolute temperature, and R is the gas constant. To evaluate g_{23}, we must first know the solubility parameter (δ) of the PAN copolymer, which can be calculated with the help of the molar gravitational constant F of different groups in repeated units. According to the ternary solubility parameter theory suggested by Hansen, δ of the polymer can be calculated from the following equations:[21]

$$\delta_d = \sum F_{di} \Big/ \overline{V} \tag{5}$$

$$\delta_p = \sqrt{\sum F_{pi}^2} \Big/ \overline{V} \tag{6}$$

TABLE III
Contributions of Several Structural Groups to Each Component of δ

Group	F_{di} [(J cm^3)$^{1.2}$/mol]	F_{pi} [(J cm^3)$^{1.2}$/mol]	E_{hi} (J/mol)
—CH_2—	269.94	0	0
—C(—H)—	79.76	0	0
—C(—)—	−69.53	0	0
—COOH	529.66	419.23	9999.76
—CN	429.45	1100.21	2502.03

The data were taken from ref. 21.

$$\delta_h = \sqrt{\sum E_{hi}} \Big/ \overline{V} \tag{7}$$

$$\delta^2 = \delta_d^2 + \delta_p^2 + \delta_h^2 \tag{8}$$

where $\overline{V}$ is the total molar volume of all the groups included in the structural unit. δ_d is the dispersion force component, δ_p the polar force component, and δ_h the hydrogen component. F_{di}, F_{pi}, and E_{hi} are three parameters for calculating the three components of δ. The contribution of several structural groups to each component of δ is summarized in Table III.[21] In this way, the components of δ were obtained.

Following eqs. (5)–(8) and Table III, δ and its components of the PAN copolymer used in this study were computed. The δ values of the PAN copolymer and DMF are listed in Tables IV and V, respectively.[20]

According to eq. (5) and Table IV, g_{23} turned out to be equal to 0.077. The accuracy of g_{23} was secondary, for its influence on the phase diagram was insignificant.

TABLE IV
δ and Its Components for the PAN Copolymer and DMF

Solvent and copolymer	δ_d [(J/cm^3)$^{0.5}$]	δ_p [(J/cm^3)$^{0.5}$]	δ_h [(J/cm^3)$^{0.5}$]	δ [(J/cm^3)$^{0.5}$]
—CH_2—C(COOH)(—CH_2COOH)—CH_2—CH(CN)—	16.09	18.96	8.84	26.39
DMF	17.4	13.7	11.2	24.82

TABLE V
Data for the Calculation of the Ternary Phase Diagram

Parameter	Value
Temperature (K)	298
Density of DMF (g/cm^3)	0.945
Molecular weight of DMF	73.08
Density of the PAN copolymer (g/cm^3)	1.14
Molecular weight of PAN	80,000
g_{12}	$0.218 + 0.276/(1 + 0.622\phi_2)$
g_{13}	1.95
g_{23}	0.077

The data were taken from ref. 20.

Binodal curve

The Gibbs free energy of mixing (ΔG_m) of a ternary polymer solution is defined as follows:[12]

$$\frac{\Delta G_m}{R \cdot T} = n_1 \ln \phi_1 + n_2 \ln \phi_2 + n_3 \ln \phi_3 + g_{12} n_1 \phi_2 + g_{13} n_1 \phi_3 + \chi_T n_1 + g_{23} n_2 \phi_3 \quad (9)$$

where n_i represents the molar numbers and ϕ_i represents the volume fractions. χ_T is the ternary interaction parameter, which is often difficult to determine except to use an estimated value during the process of calculation. Then, according to the definition of chemical potential, three such equations hold for a ternary polymer solution as follows:[12]

$$\frac{\Delta\mu_1}{R \cdot T} = \ln \phi_1 + 1 - \phi_1 - \frac{v_1}{v_2} \cdot \phi_2 - \frac{v_1}{v_3} \cdot \phi_3 + (g_{12} \cdot \phi_2 + g_{13} \cdot \phi_3) \cdot (\phi_2 + \phi_3) - \frac{v_1}{v_2} g_{23} \phi_2 \phi_3 - u_1 u_2 \phi_2 \left(\frac{dg_{12}}{du_2}\right) - \phi_1 \phi_3^2 \left(\frac{dg_{13}}{d\phi_3}\right) - \frac{v_1}{v_2} \phi_2 \phi_3^2 \left(\frac{dg_{23}}{d\phi_3}\right) \quad (10)$$

$$\frac{\Delta\mu_2}{R \cdot T} = \ln \phi_2 + 1 - \phi_2 - \frac{v_2}{v_1} \phi_1 - \frac{v_2}{v_3} \phi_3 + \left(\frac{v_2}{v_1} g_{12} \phi_1 + g_{23} \cdot \phi_3\right) \cdot (\phi_1 + \phi_3) - \frac{v_2}{v_1} \cdot g_{13} \cdot \phi_1 \cdot \phi_3 + \frac{v_2}{v_1} \cdot \phi_1 \cdot u_1 \cdot u_2 \cdot \left(\frac{dg_{12}}{du_2}\right) - \frac{v_2}{v_1} \phi_1 \phi_3^2 \left(\frac{dg_{13}}{d\phi_3}\right) - \phi_2 \phi_3^2 \left(\frac{dg_{23}}{d\phi_3}\right) \quad (11)$$

$$\frac{\Delta\mu_3}{R \cdot T} = \ln \phi_3 + 1 - \phi_3 - \frac{v_3}{v_1} \cdot \phi_1 - \frac{v_3}{v_2} \cdot \phi_2 + \left(\frac{v_3}{v_1} \cdot g_{13} \cdot \phi_1 + \frac{v_3}{v_2} g_{23} \phi_2\right)(\phi_1 + \phi_2) - \frac{v_3}{v_1} g_{12} \phi_1 \cdot \phi_2 + \phi_3 \left[\frac{v_3}{v_1} \phi_1 \left(\frac{dg_{13}}{d\phi_3}\right) + \frac{v_3}{v_2} \phi_2 \left(\frac{dg_{23}}{d\phi_3}\right)\right](\phi_1 + \phi_2) \quad (12)$$

where v_i denotes the molar volume of component i, $\Delta\mu_i$ (i = 1, 2, 3) is the difference between the chemical potential of component i in the mixture and pure state. $u_1 = \phi_1/(\phi_1 + \phi_2)$, and $u_2 = \phi_2/(\phi_1 + \phi_2)$. On the basis of the definition of the binodal curve, the chemical potential of the polymer-rich phase and that of the polymer-lean phase achieve equilibrium:

$$\Delta\mu_{i,A} = \Delta\mu_{i,B}, \quad i = 1, 2, 3 \quad (13)$$

In addition, the components in the two phases obey the material conservation equations:

$$\sum \phi_{i,A} = \sum \phi_{i,B} = 1, \quad i = 1, 2, 3 \quad (14)$$

Equations (10)–(14) include five coupled nonlinear equations with six unknowns: $\phi_{1,A}$, $\phi_{2,A}$, $\phi_{3,A}$, $\phi_{1,B}$, $\phi_{2,B}$, and $\phi_{3,B}$. If one of them is chosen as an independent value, they can be determined with a set of interaction parameters.

Spinodal curve

The spinodal of ternary systems satisfies the following equation:[22]

$$G_{22} \cdot G_{33} = (G_{23})^2 \quad (15)$$

The free energies G_{22}, G_{23}, and G_{33} may be written as follows:

$$G_{22} = \frac{1}{\phi_1} + \frac{v_1}{v_2 \phi_2} - 2g_{12} + 2(u_1 - u_2)\left(\frac{dg_{12}}{du_2}\right) + u_1 u_2 \left(\frac{d^2 g_{12}}{du_2^2}\right) \quad (16)$$

$$G_{23} = \frac{1}{\phi_1} - (g_{12} + g_{13}) + \frac{v_1}{v_2} g_{23} + u_2(u_1 - 2u_2)\left(\frac{dg_{12}}{du_2}\right) + u_1 u_2^2 \left(\frac{d^2 g_{12}}{du_2^2}\right) - \phi_3 \left(\frac{dg_{13}}{d\phi_3}\right) + \frac{v_1}{v_2} \phi_3 \left(\frac{dg_{23}}{d\phi_3}\right) \quad (17)$$

$$G_{33} = \frac{1}{\phi_1} + \frac{v_1}{v_3} \frac{1}{\phi_3} - 2g_{13} - 2u_2^2(1 - u_1)\left(\frac{dg_{12}}{du_2}\right) + u_1 u_2^3 \left(\frac{d^2 g_{12}}{du_2^2}\right) + 2(\phi_1 - \phi_3)\left(\frac{dg_{13}}{d\phi_3}\right) + \phi_1 \phi_3 \left(\frac{d^2 g_{13}}{d\phi_3^2}\right) + \frac{2v_1}{v_2} \phi_2 \left(\frac{dg_{23}}{d\phi_3}\right) + \frac{v_1}{v_2} \phi_3 \phi_2 \left(\frac{d^2 g_{23}}{d\phi_3^2}\right) \quad (18)$$

Still, the components of the ternary system obey the material conservation equation:

$$\sum \phi_i = 1, \quad i = 1, 2, 3 \quad (19)$$

On the basis of eqs. (15)–(19), the spinodal curve is again obtained by the choice of one of the parameters as an independent variable.

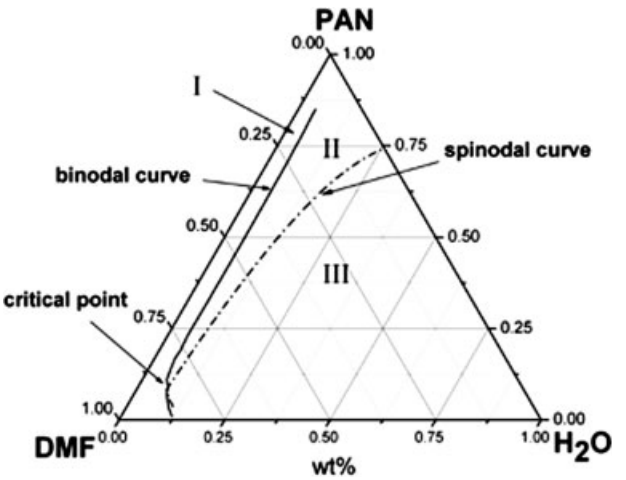

Figure 3 Theoretical binodal and spinodal curves for the H_2O–DMF–PAN system (temperature = 25°C).

Algorithm description

Altena and Smolders[22] computed the ternary phase diagram by calculating the minimum of the objective function with the least squares method. Here, we define the objective function of the binodal curve (F) as follows:

$$F = \sum f_i^2 \tag{20}$$

where $f_1 = \Delta\mu_{1,A} - \Delta\mu_{1,B}$, $f_2 = \frac{v_1}{v_2}(\Delta\mu_{2,A} - \Delta\mu_{2,B})$, and $f_3 = \frac{v_1}{v_3}(\Delta\mu_{3,A} - \Delta\mu_{3,B})$. We defined the objective functions of the spinodal curve as follows:

$$f_1 = (G_{23})^2 - G_{22} \cdot G_{33} \tag{21}$$

$$f_2 = 1 - \phi_1 - \phi_2 - \phi_3 \tag{22}$$

We used Matlab 7.0 (Mathworks, Natick, MA) to compute the phase diagram of the H_2O–DMF–PAN ternary system. Because the amount of PAN in the polymer-lean phase was very small, we assumed $\phi_{3,B}$ was negligible. The initial composition of the polymer-rich phase is supposed to be a point on the ternary phase diagram that is close to the PAN side on the PAN–H_2O axis, and the initial composition of the polymer-lean phase close to the H_2O side.

Phase diagram for the H_2O–DMF–PAN ternary system

The parameters needed for the calculation of the phase diagram for the H_2O–DMF–PAN ternary system are listed in Table V.

Figure 3 illustrates the theoretical binodal curve, spinodal curve, and the critical point (the crossing point of the two curves) for the H_2O–DMF–PAN system. The ternary phase diagram is divided into three regions by the binodal curve and the spinodal curve, respectively. Region I is the homogeneous phase region, also called the *miscible region*. Region II and region III are the metastable and unstable regions, respectively. The critical polymer composition corresponding to the critical point is significant in that it determines the mechanism of the liquid–liquid demixing. If liquid–liquid demixing occurs in a PAN solution whose composition is above the critical point, primary nuclei will form in the polymer-lean phase. Droplets containing solvent, nonsolvent, and a bit of polymer disperse in the polymer-rich continuous phase and are driven to grow by the concentration gradient until the polymer-rich continuous phase solidifies through crystallization, gelation, or vitrification.[23] Otherwise, the primary nuclei in the polymer-rich phase form, and droplets of polymer-rich solution disperse in the polymer-lean continuous phase. Also driven by the concentration gradient, these droplets continue to grow until the polymer-lean continuous phase solidifies. Right at the critical composition, the liquid–liquid demixing occurs at the unstable region (termed the *spinodal decomposition*) right at the critical composition, mechanically coherent bicontinuous structure, in which the polymer-rich and polymer-lean phases interpenetrate each other and form rapidly.

Figure 4 shows the comparison of the theoretical binodal curve with the cloud-point curve. Boom et al.[2] reported that polydisperse polymer could cause the cloud-point curve not to coincide with the binodal curve completely. In Figure 4, the low-concentration part of the theoretically calculated binodal curve is in good agreement with the experimentally determined cloud-point curve, which takes into

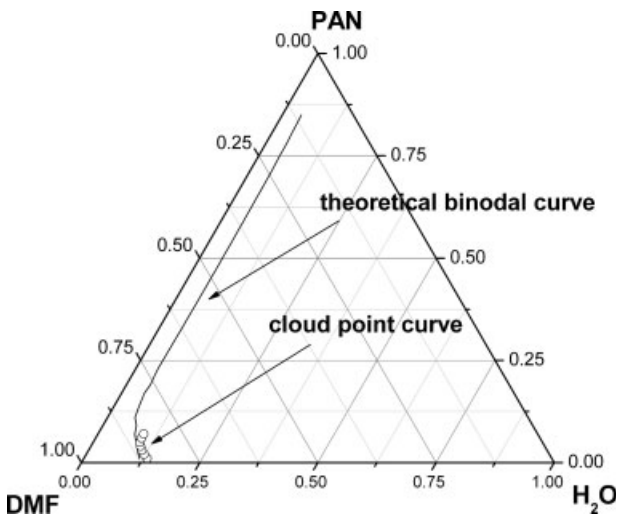

Figure 4 Comparison of the theoretical bimodal curve and the cloud-point curve.

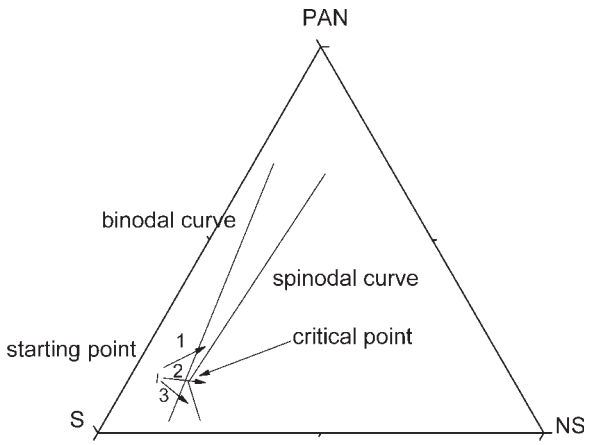

Figure 5 Schematic phase diagram of a ternary system consisting of a nonsolvent (NS), a solvent (S), and a polymer.

account the polydispersity of the PAN copolymer used and the experimental errors.

Figure 5 depicts the schematic phase diagram of another ternary system. The starting point represents the initial composition of the PAN solution; three arrows point to different changing routes of the composition in the ternary system. Arrow 1 reveals the growth of the concentrations of both PAN and the nonsolvent. Arrow 2 shows that the content of the solvent fell, whereas that of the nonsolvent grew, and the concentration of PAN remained almost constant. As for arrow 3, the concentrations of both PAN and the solvent decreased with increasing nonsolvent. It is known that after a spinning solution is extruded from spinneret, it enters a coagulating bath to form nascent fibers. During the formation of the fiber structure, double diffusion leads to a decrease in the composition of the solvent in the spinning solution and an increase in that of the nonsolvent. However, because the outer part of the fiber solidifies more quickly, as that is where the double diffusion initiates, a polymer-rich fiber skin with a denser structure forms, a consequence resulting from route 1 and termed *instantaneous phase separation*. On the other hand, as the rate of the double diffusion abates when it moves toward inside the fiber, the inner part of the fiber tends to solidify more slowly so that a polymer-lean core with a loose structure forms. This phenomenon corresponds to route 3, and we call it *delayed phase separation*. Because the outer part and inner part of the fiber undergo such phase separations with different solidification rates, the macromolecular chains of the PAN tend to migrate from the inner part out, which accelerates the formation of the skin–core structure. PAN fibers with a skin–core structure have relatively poor mechanical properties because of such inhomogeneity in the whole fiber.

If the starting composition approaches the critical point, the PAN solution may jump to the unstable region without passing through the metastable region along route 2. Liquid–liquid demixing will then take place spontaneously, which leads to an interpenetrating bicontinuous structure. In this case, the resulting fiber is homogeneous and possesses good mechanical properties.

Analysis of the PAN fiber

The mechanical properties of the as-spun PAN fibers produced from PAN/DMF solutions with different H_2O contents are listed in Table VI. With the increase of H_2O content in the PAN spinning solution, both the tenacity and Young's modulus of the resultant fibers rose first and then decreased. Figure 6 shows the scanning electron micrographs of the cross sections of the PAN fibers. The number of the fingerlike pores on the cross section first decreased and then increased with H_2O content. Also, the skin–core structure became less apparent when the H_2O content increased from 0 to 3 wt %. When H_2O continued to rise from 3 to 5 wt %, there was little change in the skin–core structure. These phenomena were not surprising when we considered the thermodynamic behavior of the PAN solution during fiber formation, as discussed previously. The composition of the PAN solution with 3 wt % H_2O was near the critical point in the phase diagram, and it may have entered the unstable region following a route very close to route 2, shown in Figure 5. Consequently, the resultant fiber had a comparatively homogeneous cross section with few fingerlike pores and exhibited better mechanical properties. The compositions of the PAN solutions without and with 1 wt % H_2O were relatively far from the critical point, and they may have entered the metastable region. The formed fibers thus had a cross section with more pores and skin–core structure. For the PAN solution with 5 wt % H_2O, the composition may have been so close to the critical point that the solution underwent liquid–liquid demixing or gelled to some extent before fiber formation, which explains the increased pores on the cross section and the reduced tenacity and Young's modulus of the as-spun fibers.

TABLE VI
Mechanical Properties of the As-Spun PAN Fibers Produced from Different PAN Solutions

Sample	Tenacity (cN/dtex)	Young's modulus (cN/dtex)
0 wt % H_2O	0.85	10.53
1 wt % H_2O	0.96	12.28
3 wt % H_2O	1.13	15.08
5 wt % H_2O	1.04	14.70

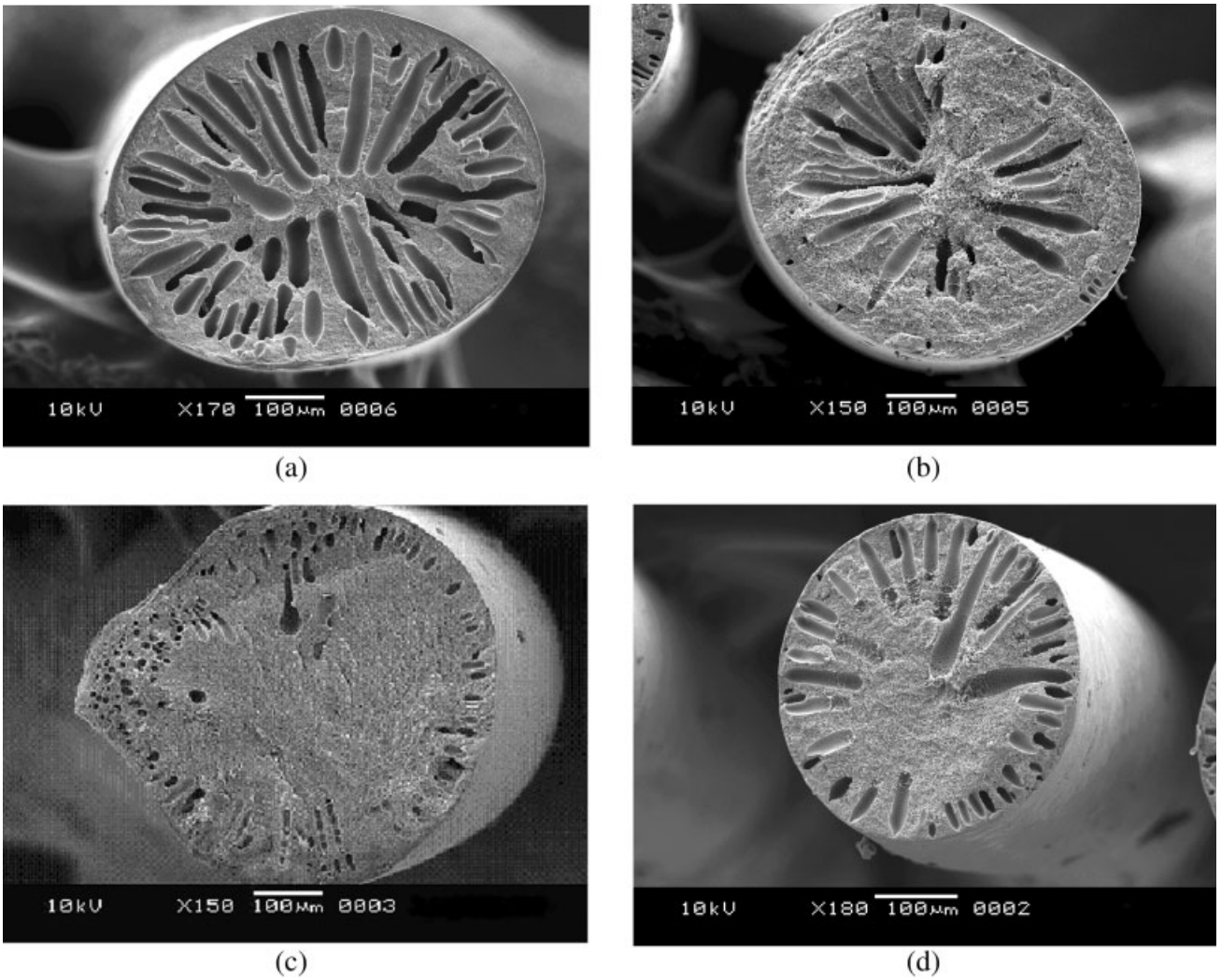

Figure 6 Scanning electron micrographs of cross sections of PAN fibers produced from PAN solutions containing (a) 0, (b) 1, (c) 3, and (d) 5 wt % H_2O.

CONCLUSIONS

The cloud-point curve for a ternary system of H_2O–DMF–PAN was obtained with the method of cloud-point titration. The theoretical phase diagram was determined by numerical calculation on basis of the extended Flory–Huggins theory. First, the equilibrium swelling experiment was used to effectively determine g_{13}. g_{12} was then derived as a function of ϕ_2, and the value of g_{12} remained below 0.5 in the whole range of ϕ_2, which indicated a strong interaction between H_2O and DMF. g_{23} was obtained with the Hildebrand formula. The low-concentration part of the experimental cloud-point curve was in good agreement with the theoretical binodal curve when the polydispersity of PAN and the experimental errors were considered.

From the phase diagram for the ternary system of H_2O–DMF–PAN thus obtained, we determined that if the PAN composition in the solution was at the critical point defined in the phase diagram, liquid–liquid demixing following spinodal decomposition occurred in the unstable region, where the solution was coagulated and an interpenetrating bicontinuous structure formed in the fiber, which led to a uniform fiber morphology. The mechanical properties and cross-section morphology of the as-spun PAN fibers produced from the PAN solutions containing different amounts of H_2O were analyzed. The experimental results verify the formation mechanisms of the PAN fiber derived from the theoretical phase diagram. Therefore, the appropriate PAN composition in a spinning solution is the prerequisite to the prevention of the skin–core structure and the achievement of PAN fibers with a homogeneous morphology and good mechanical properties.

References

1. Chen, L.; Shen, X. Membr Sci Technol 1997, 17, 1.
2. Boom, R. M.; Boomgaard, T.; van den Berg, J. W. A.; Smolder, C. A. Polymer 1993, 34, 2348.

3. Sadeghi, R.; Ziamajidi, F. Fluid Phase Equilib 2007, 255, 46.
4. Garcia-Lopera, R.; Monzo, I. S.; Abad, C.; Campos, A. Eur Polym J 2007, 43, 231.
5. Benabdelghani, Z.; Etxeberria, A.; Djadoun, S.; Iruin, J. J.; Uriarte, C. J Chromatogr A 2006, 1127, 237.
6. Wei, Y. M.; Xu, Z. L.; Yang, X. T.; Hong, L. L. Desalination 2006, 192, 91.
7. Melad, O.; Mark, J. E. J Macromol Sci Phys 2005, 44, 833.
8. James, J.; Vellaichami, S.; Krishnan, R. S. G.; Samikannu, S.; Mandal, A. B. Chem Phys 2005, 312, 275.
9. Haghtalab, A.; Mokhtarani, B. Fluid Phase Equilib 2004, 215, 151.
10. Chang, L. L.; Woo, E. Polym Int 2003, 52, 249.
11. Silva, G. A.; Eckelt, J.; Goncalves, M. C.; Wolf, B. A. Polymer 2003, 44, 1075.
12. Tompa, H. Polymer Solutions; Butterworths: London, 1956.
13. Jun, S.; Quan, Y.; Cong, G. Membrane Technical Manual; Chemical Industry: Beijing, 2001.
14. Yilmaz, L.; McHugh, A. J. J Appl Polym Sci 1986, 31, 997.
15. Koningsveld, R.; Kleintjens, L. A. Macromolecules 1971, 4, 637.
16. Young, T. H.; Chuang, W. Y. J Membr Sci 2002, 210, 349.
17. Mulder, M. Fundamentals of Membrane Technology; Tsinghua University Press: Beijing, 1997; pp 62 and 84.
18. Van de Witte, P.; Dijkstra, P. J.; Berg, J. W. A.; Feijen, J. J Membr Sci 1996, 117, 1.
19. Zeman, L.; Tkacik, G. J Membr Sci 1988, 36, 119.
20. Wypych, G. Solvent Manual; China Petrochemical Industry: Beijing, 2002.
21. Borun, L. Polymer Physics; China Textile: Beijing, 2000.
22. Altena, F. W.; Smolders, C. A. Macromolecules 1982, 15, 1491.
23. Bashier, L. J Polym Sci Part B: Polym Phys 1992, 30, 1299.